Experimental and numerical study of a PCM solar air heat exchanger and its ventilation preheating effectiveness

Hu, Y.; Heiselberg, P.K.; Johra, H.; Guo, R.

Published in:
Renewable Energy

DOI (link to publication from Publisher):
10.1016/j.renene.2019.05.115

Publication date:
2020

Document Version
Publisher's PDF, also known as Version of record

Renewable Energy 145 (2020) 106–115

Contents lists available at ScienceDirect

Renewable Energy

journal homepage: www.elsevier.com/locate/renene

Experimental and numerical study of a PCM solar air heat exchanger and its ventilation preheating effectiveness

Yue Hu*, Per Kvols Heiselberg, Hicham Johra, Rui Guo

Aalborg University, Division of Architectural Engineering, Department of Civil Engineering, Thomas Manns Vej 23, DK-9220 Aalborg Øst, Denmark

ARTICLE INFO

Article history:
Received 15 January 2019
Received in revised form
8 May 2019
Accepted 28 May 2019
Available online 31 May 2019

Keywords:
Renewable energy
Phase change material
Latent heat storage
Building energy conservation
Solar air heat exchanger

ABSTRACT

This article presents a PCM solar air heat exchanger integrated into ventilated window developed to maximize the use of the solar energy to pre-heat the ventilated air. The system is designed to improve the indoor air quality and thermal comfort by continuous pre-heated air supply at a reduced energy use through the capturing and storing of solar energy. This study examines the thermodynamic behavior of the system both experimentally and numerically. This entails a full-scale experiment in climate boxes to study the thermal storage and heat release ability of the facility. Accordingly, a numerical model combining heat transfer and buoyancy derived laminar flow and nonlinear thermal properties of the PCM is built and validated with the experimental data. The model is then used for configuration optimization of the PCM solar air heat exchanger to maximize the solar energy storage and the ventilation pre-heating effectiveness. The results show that for a 6-h solar charging period, the optimum PCM plate depth is 90 mm and the optimum air gap thickness is 6 mm. The same configuration can be used for both summer night cooling and winter solar energy storage applications. The total stored/released latent heat after one charging period is 93.31 MJ/m^3.

1. Introduction

Building energy use for ventilation and HVAC systems amount to more than one-third of the total energy use in industrial countries [1] and about 40% of the total energy use in Europe [2], and it shows growing trends as a result of increased thermal comfort requirements and climate changes. It has become a burden to the environment and the fossil fuel resources. To diminish the fuel consumption and carbon dioxide emission caused by building energy use, it is necessary to implement innovative technical solutions and renewable energy resources in the built environment. Many researchers have studied renewable energy such as solar energy applied in building energy systems to reduce the traditional building energy use. Excess renewable energy is often stored in thermal energy storage (TES) facilities with the advantages of grid peak shifting, building energy conservation, and the building thermal mass level improvement.

Phase change material (PCM) applied in TES is one of the most promising solutions for renewable energy storage and has recently drawn much attention within the scientific community [3]. Unlike the materials with only sensible energy storage, PCM releases/absorbs large amounts of latent heat during its phase transition in a small temperature range. The heat capacity of PCM during the phase transition period is much higher than the conventional building materials. The high energy density of the PCM offers a large heat storage ability with a relatively small storage volume, which makes it a good candidate for TES [4]. With adequate design and choices, the phase transition of the material occurs within the range of indoor thermal comfort, which allows direct applications of PCM in the building environment [5–7].

Ventilative heating or cooling systems integrating PCM for thermal storage is a common building application, which several research groups have tested and studied. For example, ventilation night cooling during a warm summer discharges PCM units at nighttime (cold storage) and then utilize these units during daytime to cool down the hot outdoor air used as ventilation inlet air [8–11]. Some other strategies focus more on power load peak shaving and demand shifting. For instance, Labat et al. [12] designed a PCM-to-air heat exchanger storage for heating, ventilation, air conditioning (HVAC) systems to shift the cooling demand from high to low electricity price periods. The PCM is discharged (cooled down) by the HVAC systems during low electricity price

* Corresponding author.
E-mail address: hy@civil.aau.dk (Y. Hu).

https://doi.org/10.1016/j.renene.2019.05.115

Nomenclature

Symbols

ρ	density of material [kg/m^3]
Cp	specific heat capacity [J/(kg K)]
T	temperature [°C]
t	time [s]
k	thermal conductivity [W/(m K)]
Q	heat source [W/m^3]
q	heat flux [W/m^2]
q_1	solar radiation [W/m^2]
q_2	natural convection heat flux [W/m^2]
$\overline{h}$	average heat transfer coefficient [W/(m^2·K)]
T_{ext}	temperature in cold box [°C]
$\overline{Nu}_L$	average Nussle number [dimensionless]
L	vertical length of PCM plates [m]
Ra_L	local Rayleigh number [dimensionless]
Pr	Prandtl number [dimensionless]
Gr_L	local Grashof number [dimensionless]
g	gravity acceleration [m/s^2]
α	thermal expansion coefficient [1/K]
μ	dynamic viscosity [Pa s]
u	velocity [m/s]
p	absolute pressure [Pa]
F	buoyancy force [N/m^3]
M	molar mass [kg/mol]
R	universal gas constant [J/(mol K)]

periods. The discharged PCM is then used during high price periods to decrease the energy demand for cooling. In winter time, PCM can be used directly [13–15] or indirectly [16–18] with solar energy systems or as TES integrated with other heating systems such as heat pump [19], floor heating [20], and ceiling heating [21]. Studies have shown that the integration of PCM in the building environment can significantly increase the building heat storage capacity and, thereby, improve the indoor space heating energy flexibility and ease the building demand-side management [22,23]. De Gracia et al. tested a ventilated double skin facade with PCM in the air cavity for both cooling [24] and heating [25] purposes. They found out that such PCM ventilation system can effectively prevent overheating in summer and reduce the electrical consumption of the HVAC system in winter.

Solar collectors can be used for providing pre-heated air to ventilation systems. The traditional solar air collector consists of an absorber and a transparent glass, and it facilities airflow inside the collector. Applications for solar collectors can be found in drying systems for agriculture [26] and marine [27] products, packed bed thermal storage unit [28], as well as space heating systems [29–31]. Nevertheless, a large heat transfer area and high flow rates are required for good performances because of the low thermal capacity and thermal conductivity of the air and the low convection coefficient on the surface of the absorber [32]. Applying PCM to the solar-air collector system has the advantage of more thermal energy storage, longer thermal release time [33], and more stable pre-heated air temperature [34]. However, the conventional method to apply PCM into a solar collector system is to use the material as the heat storage medium in the storage tank. The heat transfer fluid between the solar collector and the PCM heat storage tank is usually water. The PCM in this system always has a relatively high phase change temperature (around 40–60 °C) [35].

This paper proposes a different solution to apply PCM into the building energy system. It includes a double glazing ventilated window and a PCM heat exchanger. The system is designed to improve the indoor air quality and thermal comfort by continuous pre-heated air supply at a reduced energy use through the capturing and storing of solar energy. The double glazing window works as a trombe wall during the daytime when solar radiation is available. The PCM solar air heat exchanger directly stores the heat from the solar radiation and releases the heat later when solar radiation is less available to pre-heat the ventilated air. It has a smaller volume compare to the conventional PCM tank. The PCM in the solar-air heat exchanger has a phase change temperature around room temperature, which is good for the indoor thermal comfort. The relatively thin PCM plates compensate for the low thermal conductivity of the PCM and make the heat store and release processes faster.

This paper will experimentally and numerically study the thermal behavior of the PCM solar air heat exchanger and optimize its configuration to achieve the highest energy efficiency of the system. For that purpose, a full-scale laboratory experiment for testing the PCM solar air heat exchanger is conducted. Later on, the paper presents a numerical model accounting for the heat transfer and buoyancy effects in the solar air heat exchanger. The model is validated by the experimental data. Finally, the verified model is used to optimize the configuration of the PCM heat exchanger, including the depth of the PCM plates and the air gap thickness between PCM plates.

2. System description

Fig. 1 presents the configuration of the ventilated window with the PCM solar air heat exchanger. The ventilated window is a double glazing window with an air cavity between the two glazing layers, which allows ventilated air to go through. The solar air heat exchanger is made of parallel PCM plates separated by thin air gaps. The PCM plates are mounted in a wood frame with a glass on the front surface. There are openings on the top and bottom of the PCM heat exchanger frame and on the top of the ventilated window, to enable the ventilation of air through the system.

The system is designed to improve the indoor air quality and thermal comfort by continuous pre-heated air supply at a reduced energy use through the capturing and storing of solar energy. Fig. 2 illustrates the operation strategy of the ventilated window system in winter or transition seasons. In the daytime, the system is in solar energy storage mode (see Fig. 2(a)). The solar radiation charges the PCM in the solar air heat exchanger when solar energy is available. The ventilation air only passes the ventilated window and is heated up by the solar radiation, before it enters the indoor room. The ventilation pre-heating mode is on when the solar radiation is less than 200 W/m^2, as seen in Fig. 2(b). The cold ambient air passes the solar air heat exchanger from the bottom, and the stored heat heats it up. Then the pre-heated air passes through the double glazing window into the indoor space. The ventilation bypass mode is on when there is a cooling need in the space, and the inlet air temperature from the window system should be close to the outdoor air temperature, and at a maximum the airflow rate, as seen in Fig. 2(c).

With the new solar air heat exchanger ventilation system, solar energy and the PCM solar storage preheat the ventilation air to make the most use of the solar energy and to increase the inlet air temperature and thermal comfort in winter. It can benefit both the buildings under renovation and the new buildings. In building

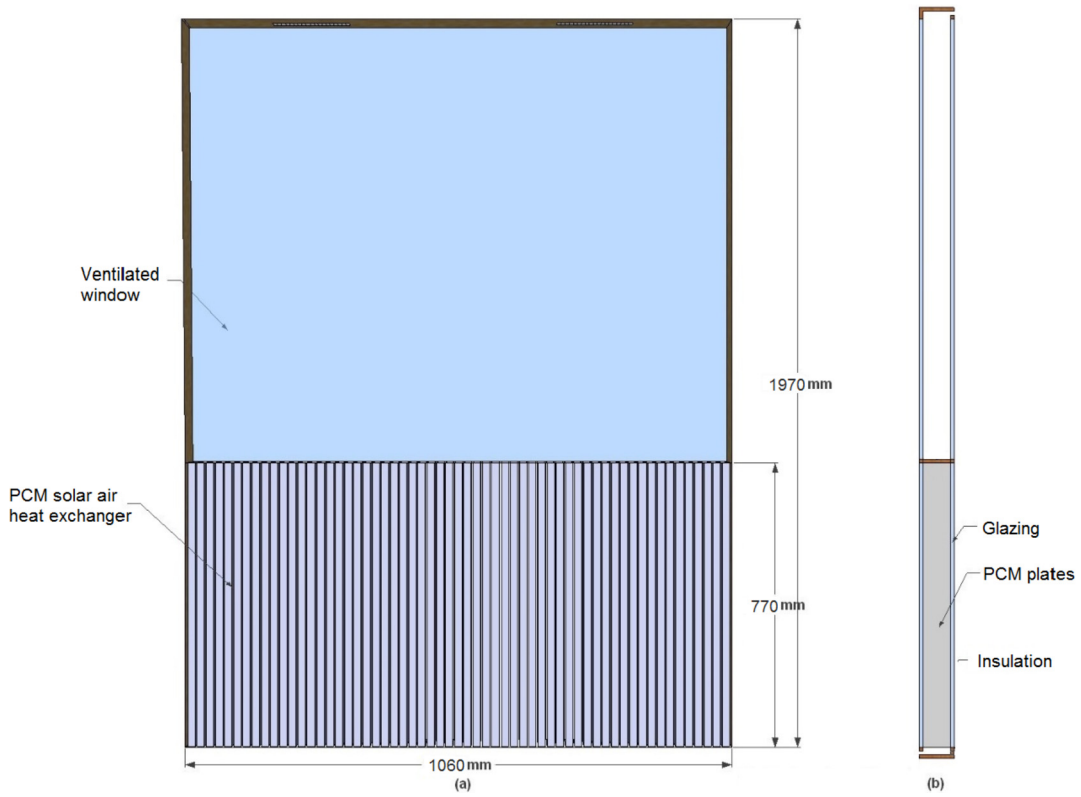

Fig. 1. Description of the ventilated window with PCM heat exchanger [36]. (a) Front view; (b) Side view.

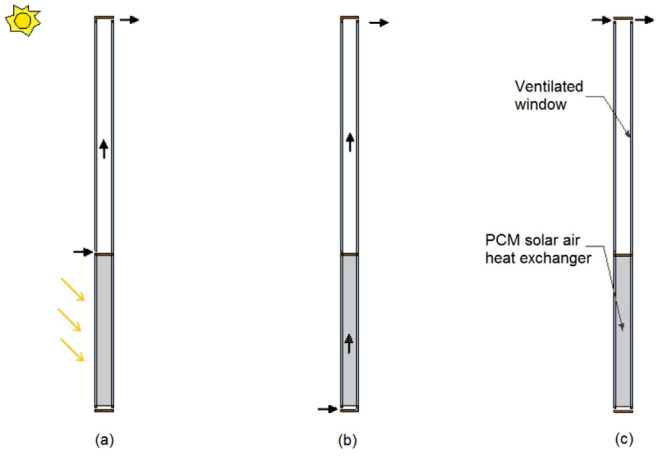

Fig. 2. System operation strategy (a) solar energy storage mode; (b) ventilation pre-heating mode; (c) ventilation bypass mode.

renovation, the install an efficient ventilation system with heat recovery is a challenging work. The application of the presented system can be an alternative method to ensure an energy efficient ventilation solution in these buildings. Moreover, the installation of the application only requires some façade envelope reconstruct. The easy installation of the system makes it good for the building renovation projects. For new buildings with decentralized ventilation solutions, the system can contribute to improve the energy efficiency of the buildings by better capture and utilization of the solar energy. The solar energy added into the building energy system is used to cover the heat demand of the buildings. As a result, the building energy consumption is reduced.

3. Experimental setup

The heat storage and heat release processes of the solar air heat exchanger are tested with a full-scale experiment in a *Hot Box* and *Cold Box* setup in the laboratory, as shown in Fig. 3. Both of the boxes are equipped with cooling coil and electric heater. The air temperature in the cold box is controlled by proportional integral derivative (PID) controllers at $8 \pm 1\,^{\circ}C$. A ventilation system connects the two boxes and creates an under-pressure in the hot box compared to the cold box by operation of a fan in the ventilation duct. It induces an air flow from the cold box to the hot box through the solar heat exchanger. The air flow rate during the ventilation pre-heating mode is kept constant at 106 m^3/h, which is measured by the orifice plate.

An artificial sun is used to provide solar radiation. It is an assembly of 56 OSRAM Ultra-Vitalux lamps mounted on a metal frame (see Fig. 4). The lamps are in an 8×7 matrix to create an even radiant distribution to the surface of the heat exchanger. Each lamp has a power of 300 W. The radiation spectrum of the lamps is similar to the natural alpine sunlight [37]. The distance from the artificial sun to the cold box is 0.95 m.

A pyranometer, Kipp & Zonen CMP 22, is used to measure the solar radiation on the surface of the solar air heat exchanger. The measurement uncertainty is $\pm$ 2%. The temperature and radiation measurement data is collected by a Fluke Helios Plus 2287A data logger every 10 s. The average solar radiation measured on the surface of the PCM solar radiator is 550 W based on 30 evenly distributed measurement points. A slight distribution inhomogeneity can be observed between the right, left, and center parts of the solar collector. The radiation on the left side is higher than the rest of the area. The deviation between the lowest and highest radiation is 9.35%.

The air flow rate is measured by an orifice plate EHBA Ø 125 mm

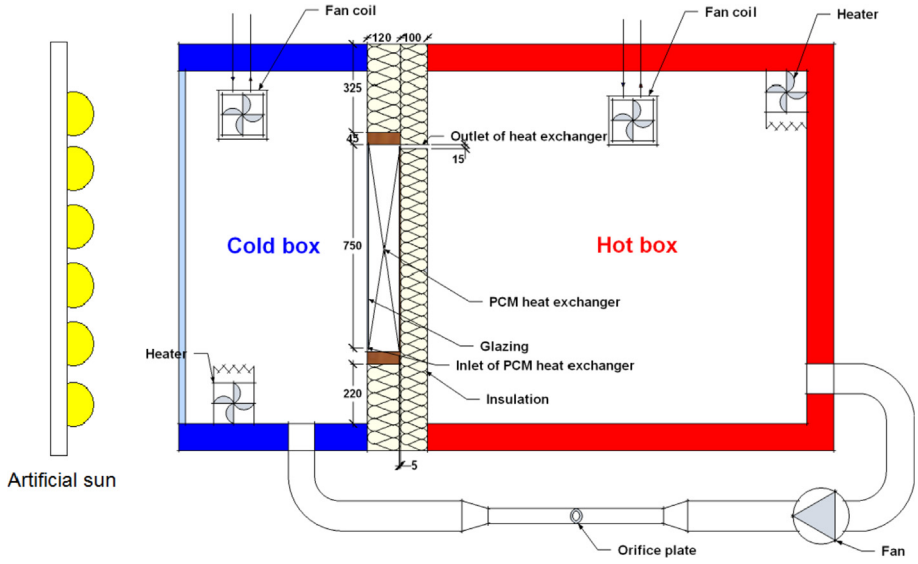

Fig. 3. Experimental setup of the solar air heat exchanger test.

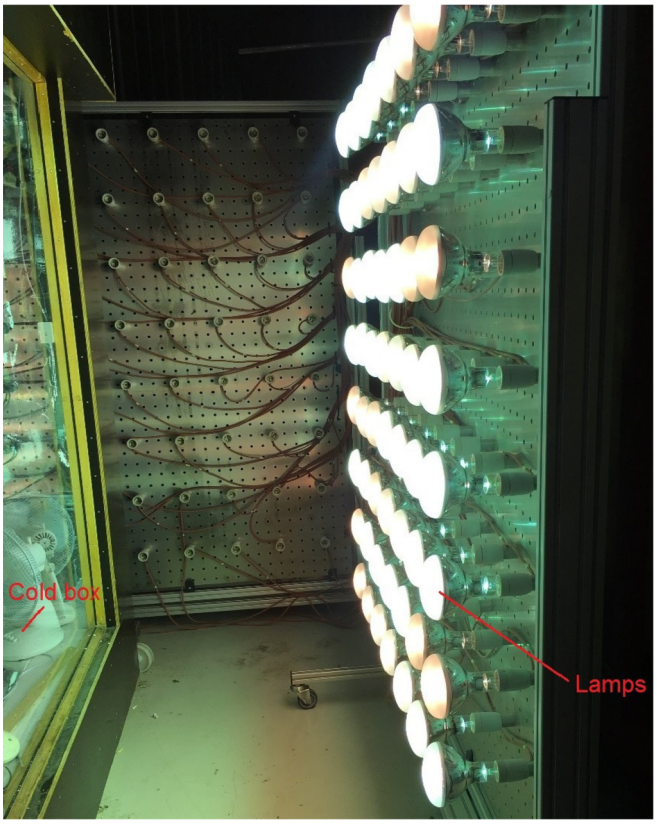

Fig. 4. The artificial sun.

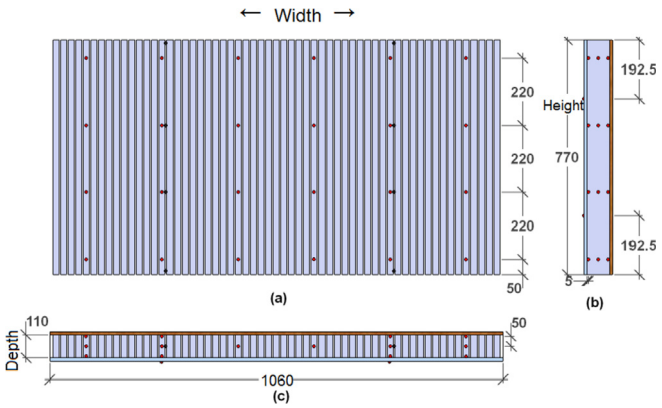

Fig. 5. Temperature measurement points in the solar air heat exchanger.

with an uncertainty of ± 7.5%. 72 calibrated type K thermocouples are used for monitoring the air and PCM temperature, as shown in Fig. 5. The temperature uncertainty is ± 0.15 K. 6 PCM plates are chosen to measure the material temperature at different heights and depths in the heat exchanger. Four of them are with 12 measurement points each, and two are with 4 measurement points each. For the air temperature measurements, the thermocouples are protected from solar radiation by mechanically ventilated silver-coated tubes (see Fig. 6).

The PCM used in the solar air heat exchanger is 50% paraffin wax impregnated fiberboard. It is a shape-stable PCM compound. The properties of the PCM compound are measured by Differential Scanning Calorimetry (DSC). The heating/cooling rate during the measurement is 0.5 °C/min for freezing and melting processes. The results show that the PCM has a melting range of 16 °C–23 °C and a freezing range of 14 °C–21.5 °C. The melting peak is at 20.7 °C, and the freezing peak is at 21.5 °C. Based on the results 0.8 °C temperature hysteresis is observed. The total heat capacity of the PCM plates is 117 kJ/kg (for a 10 °C–30 °C temperature range). More details about the measured PCM properties are available in Ref. [36]. The thickness of the PCM plates is 12.5 mm, the depth of the PCM plates is 110 mm, and the thickness of the air gaps is 6 mm in the experimental setup.

4. Numerical methods

This chapter describes the numerical methods for the heat transfer in the PCM solar air heat exchanger. Chapter 4.1 introduces the numerical model. Chapter 4.2 is the validation of the model with experimental data.

Fig. 6. Measurement of air temperature in the cold box.

4.1. Model description

A 3D model is built in COMSOL Multiphysics. Symmetry boundary conditions are used to save computational time, with half of the PCM plate and half of the air cavity. The PCM plate is modeled with a heat transfer module. The fluid in the air cavity inside the heat exchanger is modeled by heat transfer conjunct laminar flow module.

Heat transfer in the PCM is considered as conduction heat transfer. The PCM is encapsulated in the cellular structure of the fiber board. It is therefore assumed that no convection takes place within the shape steady micro-encapsulated PCM plates. The governing heat equation for the thermal energy transferred by conduction is as follows:

$$\rho Cp\frac{\partial T}{\partial t}=\nabla\cdot(k\nabla T)+Q \tag{1}$$

The heat flux between the outdoor environment and the solar air heat exchanger (q) consists of the solar radiation (q_1) and the natural convection (q_2) components.

$$q=q_1+q_2 \tag{2}$$

The solar radiation q_1 is depending on the height of the measurement points on the surface of the window. It is evaluated based on the average horizontal solar radiation measured along the width of the glass surface. The solar radiation transmittance rate of the glass is 90%. The reflection and absorption of the glass are not simulated.

The convection heat flux q_2 is calculated based on Equations (3)–(7) [38].

$$q_2=\overline{h}(T_{ext}-T) \tag{3}$$

The average heat transfer coefficient $\overline{h}$ is solved base on Equation (4).

$$\overline{Nu}_L=\frac{\overline{h}L}{k}=\begin{cases}0.68+\dfrac{0.67Ra_L^{1/4}}{\left(1+(0.492/Pr)^{9/16}\right)^{4/9}} & Ra_L\le 10^9\\ \left(0.825+\dfrac{0.387Ra_L^{1/6}}{\left(1+(0.492/Pr)^{9/16}\right)^{8/27}}\right)^2 & Ra_L\ge 10^9\end{cases} \tag{4}$$

Where the local Rayleigh number Ra_L is defined by Equation (5).

$$Ra_L=Gr_LPr \tag{5}$$

Where

$$Gr_L=\frac{\rho^2 g\alpha Cp}{\mu k}\Delta TL^3 \tag{6}$$

$$Pr=\frac{Cp\mu}{k} \tag{7}$$

For the fluid flow, the Navier-Stokes equations govern the motion of the fluid in the air cavities between the PCM plates [39]. For weakly compressible Newtonian fluids such as air, the momentum equation is as follows:

$$\rho\left(\frac{\partial u}{\partial t}+u\cdot\nabla u\right)=-\nabla p+\nabla\cdot\left(\mu\left(\nabla u+(\nabla u)^T\right)-\frac{2}{3}\mu(\nabla\cdot u)\right)+F \tag{8}$$

F is the buoyancy force, which is defined as:

$$F=-g\rho(T) \tag{9}$$

The continuity equation is written as:

$$\frac{\partial\rho}{\partial t}+\nabla\cdot(\rho u)=0 \tag{10}$$

$$\frac{\partial\rho}{\partial t}=\frac{\partial p}{\partial t}\frac{M}{RT}-\frac{\partial T}{\partial t}\frac{pM}{RT^2} \tag{11}$$

For the weakly compressible flow, the pressure change is neglected. The continuity equation can be written as:

$$\frac{\partial T}{\partial t}\frac{pM}{RT^2}+\nabla\cdot(\rho u)=0 \tag{12}$$

The numerical model used for the ventilation pre-heating mode is a 2D heat transfer conjunct laminar flow model which was proposed and verified in previous work [36]. The simple 2D model has a good agreement with the heat transfer process in the heat exchanger with fewer meshes and smaller computational time but a higher mesh density than a 3D model.

4.2. Model validation

Fig. 7 shows the temperature curves of PCM at different positions on the PCM plates. Each curve is an average of the measured temperatures in the same position on different PCM plates. The simulation results show good agreement with the experimental data. The average error for the PCM temperature at the outer part, middle part, and inner part of the plates is 5.95%, 1.82%, and 4.28% respectively. The error is defined in Eq. (13).

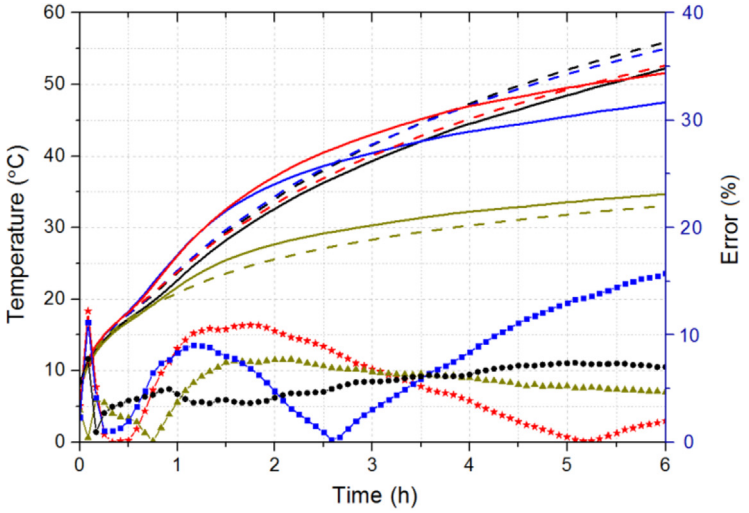

(a) PCM temperature in the outer part of the plates.

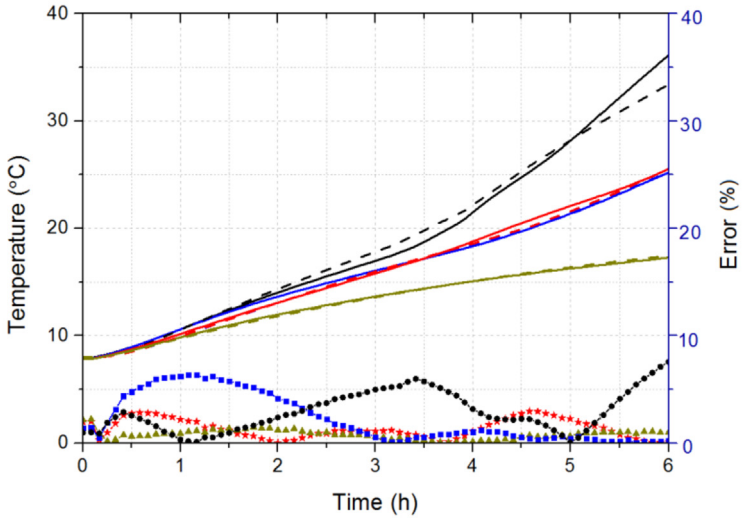

(b) PCM temperature in the middle part of the plates.

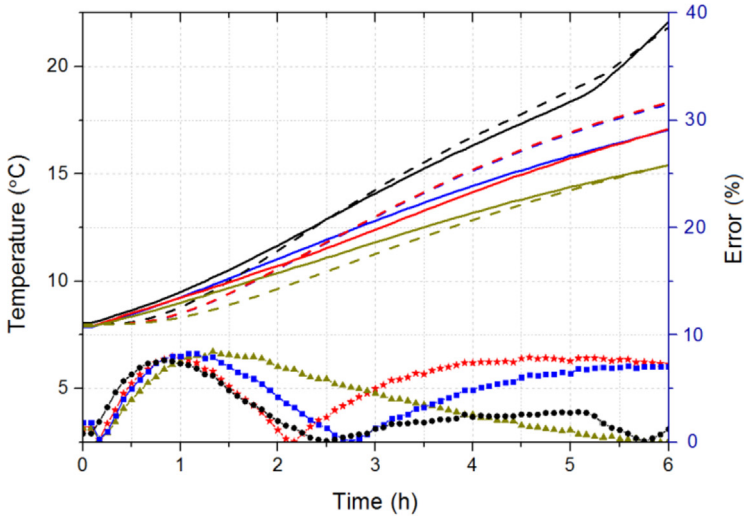

(c) PCM temperature in the inner part of the plates.

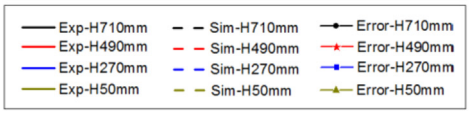

Fig. 7. Model validation with experimental data.

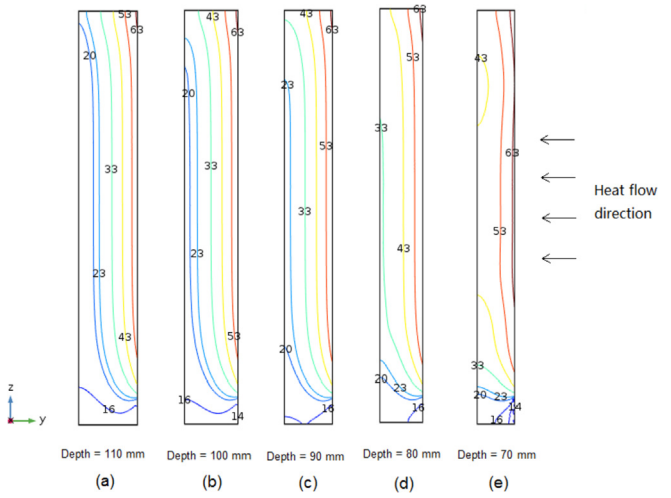

Fig. 8. Vertical PCM temperature profile in the middle of the plates after 6 h charging for different plate depths.

$$error = \left| \frac{\text{Experiment value} - \text{Simulation value}}{\text{Experiment value}} \right| \times 100\% \qquad (13)$$

5. Results and discussion

In this section, the optimized results of the depth of the PCM plates and the thickness of the air gap are presented. All the cases have an air flow rate set at 106 m^3/h. 5 cases with different plate depths are studied first. The air gap thickness is kept at 6 mm, the same as in the experimental setup. The aim of using the PCM solar air heat exchanger for ventilation preheating is to save heating energy use mainly in winter and transition seasons. The optimization is based on the energy saving potential of the PCM heat exchanger exposed to 550 W solar charging for 6 h, which is equal to the average daily radiation received in April in Denmark.

Fig. 8 shows the temperature at the vertical section in the middle of the PCM plates at time 6 h. A 550 W evenly distributed heat flow is applied to each of the PCM plates from the right side. From the temperature contours shown in Fig. 8, it can be observed that the PCM melt in the top right side of the PCM plate. The right side of the PCM starts melting first. The heat is transferred into the left side of the plate by the conduction in the PCM plates and the convection in the air gaps between the PCM plates. The area of the PCM plate with a temperature lower than 23 °C decreases with the decrease of plate depth, which indicates a higher melting fraction for a smaller PCM plate depth. However, the total volume of the PCM is decreasing with the decreasing of the PCM plate depth. Therefore, there exits an optimum PCM plate depth to maximum both the PCM melt fraction and the PCM volume in the system. The PCM at the bottom of the plate has a lower temperature because of the shelter of the inlet of the PCM heat exchanger, which prevented sunlight to reach this part. The PCM temperature is highest in the upper right corner, because of the heat flow direction and convection in the air gap between the PCM plates.

The PCM is considered fully melted (maximum latent heat storage) when its temperature rises above 23 °C base on the feature of the PCM heat capacity curve. Figs. 9 and 10 show the fraction of melted PCM and the stored latent heat for the cases with different PCM plate depths.

The PCM melt fraction is nearly maximized when the plate depth is 90 mm, and the stored latent heat is the highest for 6 h charging with 90 mm plate depth, as shown in Figs. 9 and 10. For the time period 0.5 h–5.7 h, the slopes of the curves for both melt fraction and stored latent heat are lower than for the periods 0 h–0.5 h and 5.7 h–6 h, due to the occurrence of the phase transition. The same phenomenon is observed for all the other cases. For the 70 mm and 80 mm plate depths, the PCM melt fraction reaches a constant value, meaning that the PCM in the plates is melted completely. The maximum melt fraction cannot reach 1, because the opaque insulation in the inlet of the heat exchanger in the solar energy storage mode shades the PCM plates from solar radiation at the bottom. The total PCM volume in the heat exchanger is growing with the increase of the plate depth, which increases the total thermal storage capacity. However, the charging time of the PCM increases, and the plates may not be fully melted at the end of the charging period due to the relatively low thermal conductivity of the PCM. Therefore, the melted fraction at 6 h for 100 mm and 110 mm plate depths is only 59.5% and 69.8% respectively. As a result, the stored latent heat for both depths are not the highest among all the five cases. The optimized plate depth is 90 mm with a 90.2% melt fraction for 6 h heat charging period. However, the optimized result may be different with a different heat radiation rate or charging time, which is not studied in this work.

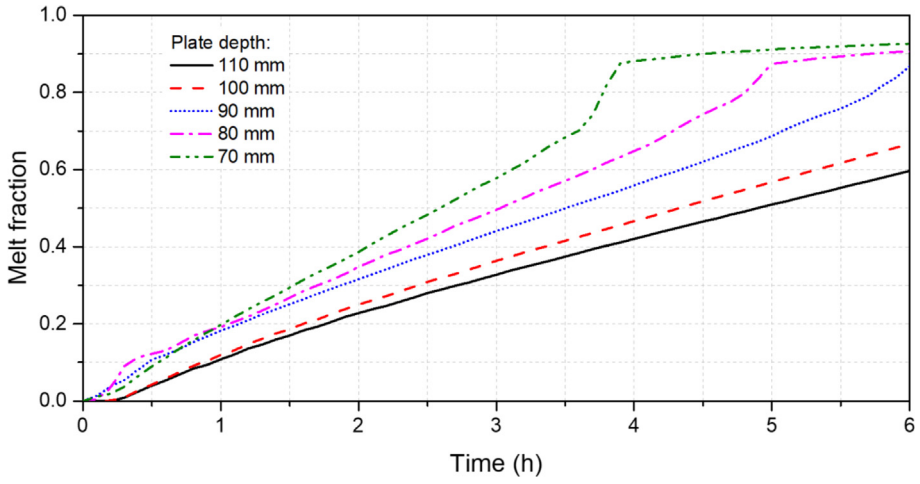

Fig. 9. The PCM melt fraction as function of time for cases with different PCM plate depths.

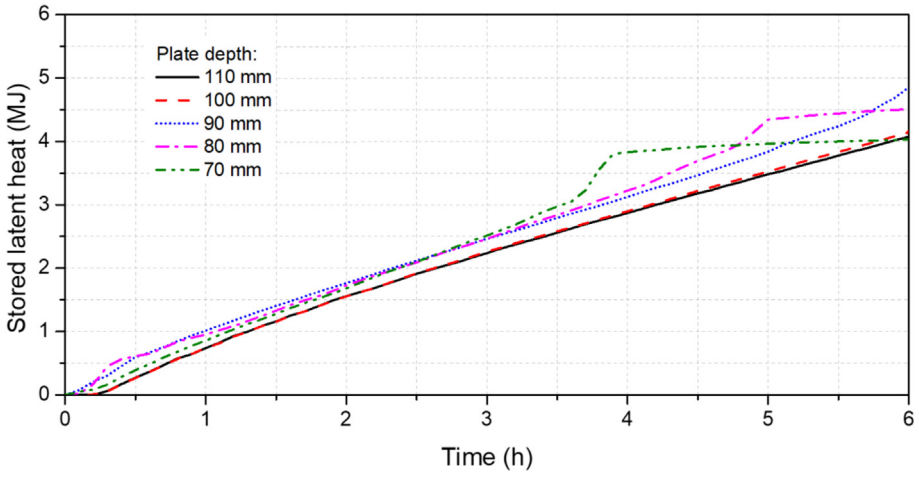

Fig. 10. The stored latent heat as function of time for cases with different PCM plate depths.

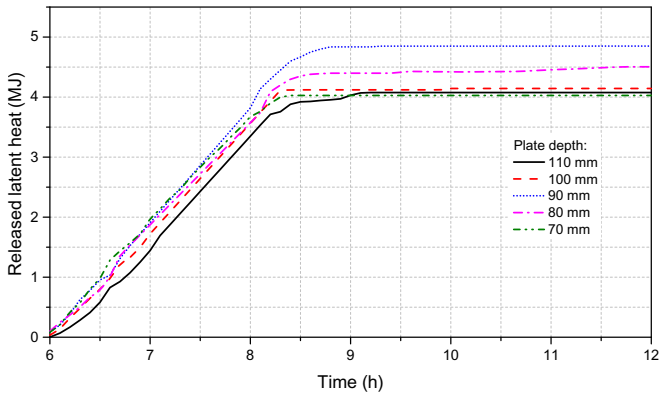

Fig. 11. The released latent heat from the PCM heat exchanger in ventilation pre-heating mode.

Fig. 11 shows the released latent heat from the PCM heat exchanger to the ventilated air when the system is in ventilation pre-heating mode. The discharge time for the energy stored are similar for all the studied cases, in the range of 2 h–3 h. It indicates that the depth of PCM plates has less influence on the discharge time. For 90 mm plate thickness, the released latent heat from the PCM to the ventilation is the highest, which is 4.85 MJ, equaling to 93.31 MJ per cube meter PCM.

The optimization of the air gap thickness in the PCM solar air heat exchanger is then investigated. 6 cases with different air gap thicknesses are compared. Fig. 12 and Fig. 13 show the results about the melt fraction and the stored latent heat of the PCM heat exchanger respectively. The total PCM volume in the solar air heat exchanger decreases with the increase of the air gap thickness, because of the fixed configuration of the PCM solar air heat exchanger available, but the PCM melting speed and charging time are improved with the increase of the air gap thickness.

As shown in Fig. 13, the stored latent heat after 6 h charging for models with 3, 4, 5, and 6 mm air gap thicknesses are similar. However, the PCM melt fraction is lower for 3, 4, and 5 mm air gap thicknesses. The optimized air gap thickness is 6 mm, which is similar to the optimum configuration for summer night ventilation (5 mm air gap thickness) with similar stored and released latent heat [36]. It indicates that the same configuration can be used for both summer night cooling and winter solar energy storage applications.

Fig. 14 shows the released latent heat from the PCM heat exchanger in ventilation pre-heating mode. The discharge rate decreases with the increase of the air gap thickness. However, the discharged time for all the cases are all in the level of 3.5 h–4 h and

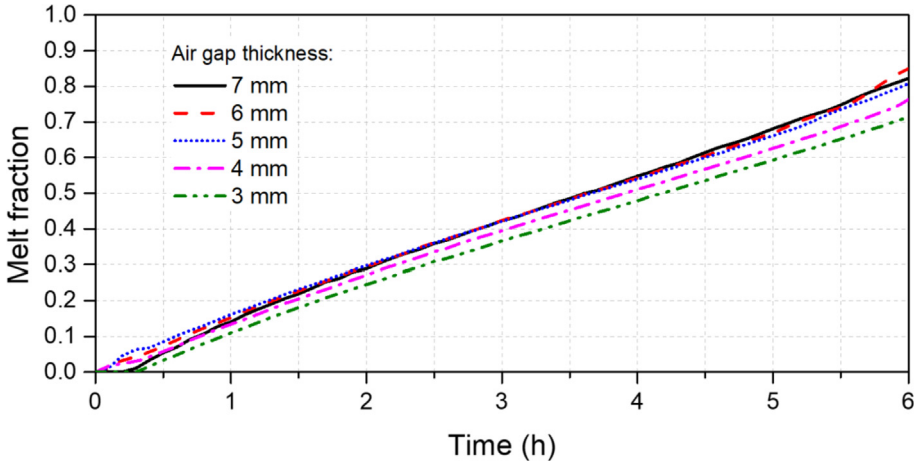

Fig. 12. The PCM melt fraction as function of time for models with different air gap thicknesses.

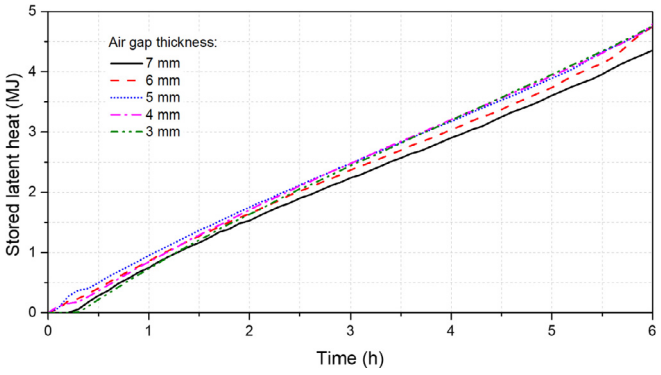

Fig. 13. The stored latent heat along with time for models with different air gap thicknesses.

numerical model with conjunct heat transfer and buoyancy driven laminar flow is built. The simulation results are in good agreement with the experimental data. Configuration optimization is conducted with different plate depths and different air gap thicknesses for a PCM heat exchanger in both the solar energy storage and the ventilation pre-heating modes. For a 6-h solar charging period, the optimum PCM plate depth is 90 mm and the optimum air gap thickness is 6 mm. The same configuration can be used for both summer night cooling and winter solar energy storage applications. The total stored and released latent heat during one charge is 93.31 MJ/m^3.

The airflow rate in the experiment and the model is higher than the required fresh air for a typical residential room. Further research should include the analysis of the air flow rate effect on the PCM discharge time. It should also include analysis in different

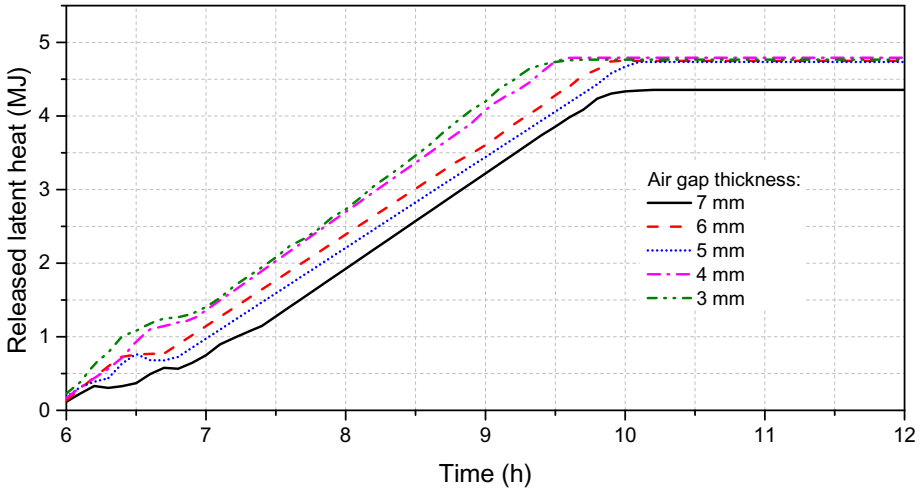

Fig. 14. The released latent heat from the PCM heat exchanger in ventilation pre-heating mode.

have no big differentials. The released energy is more related to the latent heat storage in the solar energy storage mode than to the air gap thickness.

6. Conclusions

This article presents the application of PCM into a solar air heat exchanger in a ventilated window system. Firstly, the paper introduced the configuration and working principle of the system. When solar energy is available, solar radiation charges the PCM solar air collector. The ventilation air only passes through the ventilated window to be pre-heated by solar radiation. When the solar radiation is lower than 200 W/m^2, the ventilation air passes through the PCM solar collector, where the PCM heat storage preheats it, and then the air is supplied to the room to make the most use of the captured solar energy to increase the air inlet temperature and thermal comfort in winter. In building renovation, it can be challenging to install an efficient ventilation system with heat recovery and the application of the presented system can be an alternative method to ensure an energy efficient ventilation solution in these buildings. Also, for new buildings with decentralized ventilation solutions, the system can contribute to improve the energy efficiency of the buildings by better capture and utilization of the solar energy.

This study presents a full-scale experimental test to evaluate the thermal behavior of the solar air heat exchanger. Accordingly, a climate zones to verify the optimization, and estimate the annually building energy saving potential of the system.

Acknowledgment

The EU Horizon 2020 research and innovation program under grant agreement NO. 768576(ReCO2ST) and the Chinese Scholarship Council (CSC No. 201606050118) supported this work.

References

[1] P. Heiselberg, H. Brohus, A. Hesselholt, H. Rasmussen, E. Seinre, S. Thomas, Application of sensitivity analysis in design of sustainable buildings, Renew. Energy 34 (2009) 2030–2036, https://doi.org/10.1016/J.RENENE.2009.02.016.
[2] H. Johra, P. Heiselberg, Influence of internal thermal mass on the indoor thermal dynamics and integration of phase change materials in furniture for building energy storage: a review, Renew. Sustain. Energy Rev. 69 (2017) 19–32, https://doi.org/10.1016/J.RSER.2016.11.145.
[3] M. Pomianowski, P. Heiselberg, Y. Zhang, Review of thermal energy storage technologies based on PCM application in buildings, Energy Build. 67 (2013) 56–69, https://doi.org/10.1016/j.enbuild.2013.08.006.
[4] M. Pomianowski, P. Heiselberg, R.L. Jensen, Full-scale investigation of the dynamic heat storage of concrete decks with PCM and enhanced heat transfer surface area, Energy Build. 59 (2013) 287–300, https://doi.org/10.1016/j.enbuild.2012.12.013.
[5] F. Kuznik, J. Virgone, Experimental investigation of wallboard containing phase change material: data for validation of numerical modeling, Energy Build. 41 (2009) 561–570, https://doi.org/10.1016/J.ENBUILD.2008.11.022.
[6] M. Pomianowski, P. Heiselberg, R.L. Jensen, R. Cheng, Y. Zhang, A new experimental method to determine specific heat capacity of inhomogeneous concrete material with incorporated microencapsulated-PCM, Cement Concr.

Res. 55 (2014) 22–34, https://doi.org/10.1016/J.CEMCONRES.2013.09.012.
[7] H. Johra, P. Heiselberg, Influence of internal thermal mass on the indoor thermal dynamics and integration of phase change materials in furniture for building energy storage: a review, Renew. Sustain. Energy Rev. 69 (2017) 19–32, https://doi.org/10.1016/J.RSER.2016.11.145.
[8] J. Borderon, J. Virgone, R. Cantin, Modeling and simulation of a phase change material system for improving summer comfort in domestic residence, Appl. Energy 140 (2015) 288–296. https://doi.org/10.1016/j.apenergy.2014.11.062.
[9] G. Hed, R. Bellander, Mathematical modelling of PCM air heat exchanger, Energy Build. 38 (2006) 82–89, https://doi.org/10.1016/J.ENBUILD.2005.04.002.
[10] G. Diarce, Á. Campos-Celador, K. Martin, A. Urresti, A. García-Romero, J.M. Sala, A comparative study of the CFD modeling of a ventilated active faÃ§ade including phase change materials, Appl. Energy 126 (2014) 307–317, https://doi.org/10.1016/j.apenergy.2014.03.080.
[11] M. Pomianowski, P. Heiselberg, R. Lund Jensen, Dynamic heat storage and cooling capacity of a concrete deck with PCM and thermally activated building system, Energy Build. 53 (2012) 96–107, https://doi.org/10.1016/j.enbuild.2012.07.007.
[12] M. Labat, J. Virgone, D. David, F. Kuznik, Experimental assessment of a PCM to air heat exchanger storage system for building ventilation application, Appl. Therm. Eng. 66 (2014) 375–382, https://doi.org/10.1016/j.applthermaleng.2014.02.025.
[13] S. Liu, Y. Li, Heating performance of a solar chimney combined PCM: a numerical case study, Energy Build. 99 (2015) 117–130, https://doi.org/10.1016/J.ENBUILD.2015.04.020.
[14] G. Fraisse, K. Johannes, V. Trillat-Berdal, G. Achard, The Use of a Heavy Internal Wall with a Ventilated Air Gap to Store Solar Energy and Improve Summer Comfort in Timber Frame Houses, Energy Build. 38 (2006) 293–302.
[15] F. Goia, M. Perino, V. Serra, Experimental analysis of the energy performance of a full-scale PCM glazing prototype, Sol. Energy 100 (2014) 217–233, https://doi.org/10.1016/j.solener.2013.12.002.
[16] J.F. Belmonte, M.A. Izquierdo-Barrientos, A.E. Molina, J.A. Almendros-Ibáñez, Air-based solar systems for building heating with PCM fluidized bed energy storage, Energy Build. 130 (2016) 150–165, https://doi.org/10.1016/J.ENBUILD.2016.08.041.
[17] U. Stritih, P. Charvat, R. Koželj, L. Klimes, E. Osterman, M. Ostry, V. Butala, PCM thermal energy storage in solar heating of ventilation air—experimental and numerical investigations, Sustain. Cities Soc. 37 (2018) 104–115, https://doi.org/10.1016/j.scs.2017.10.018.
[18] G. Serale, E. Fabrizio, M. Perino, Design of a low-temperature solar heating system based on a slurry Phase Change Material (PCS), Energy Build. 106 (2015) 44–58, https://doi.org/10.1016/j.enbuild.2015.06.063.
[19] J. Mazo, M. Delgado, J.M. Marin, B. Zalba, Modeling a radiant floor system with Phase Change Material (PCM) integrated into a building simulation tool: analysis of a case study of a floor heating system coupled to a heat pump, Energy Build. 47 (2011) 458–466, https://doi.org/10.1016/j.enbuild.2011.12.022.
[20] P. Devaux, M.M. Farid, Benefits of PCM underfloor heating with PCM wallboards for space heating in winter, Appl. Energy 191 (2017) 593–602, https://doi.org/10.1016/j.apenergy.2017.01.060.
[21] M. Koschenz, B. Lehmann, Development of a thermally activated ceiling panel with PCM for application in lightweight and retrofitted buildings, Energy Build. 36 (2004) 567–578, https://doi.org/10.1016/j.enbuild.2004.01.029.
[22] J.L.D. H. Johra, P. Heiselberg, Numerical analysis of the impact of thermal inertia from the furniture/indoor content and phase change materials on the building energy flexibility, in: Proc. 15th IBPSA Conf. Int. Build. Perform. Simul. Assoc. San Fr. CA, USA., n.d.
[23] H. Johra, Integration of a Magnetocaloric Heat Pump in Energy Flexible Buildings, Aalborg University, 2018. http://vbn.aau.dk/files/281673345/PHD_Hicham_Johra_E_pdf.pdf. (Accessed 4 July 2018).
[24] A. De Gracia, L. Navarro, A. Castell, Á. Ruiz-Pardo, S. Álvarez, L.F. Cabeza, Thermal analysis of a ventilated facade with PCM for cooling applications, Energy Build. 65 (2013) 508–515, https://doi.org/10.1016/j.enbuild.2013.06.032.
[25] A. De Gracia, L. Navarro, A. Castell, Á. Ruiz-Pardo, S. Alvárez, L.F. Cabeza, Experimental study of a ventilated facade with PCM during winter period, Energy Build. 58 (2013) 324–332, https://doi.org/10.1016/j.enbuild.2012.10.026.
[26] T. Koyuncu, Performance of various design of solar air heaters for crop drying applications, Renew. Energy 31 (2006) 1073–1088, https://doi.org/10.1016/J.RENENE.2005.05.017.
[27] A. Fudholi, K. Sopian, M.H. Ruslan, M.A. Alghoul, M.Y. Sulaiman, Review of solar dryers for agricultural and marine products, Renew. Sustain. Energy Rev. 14 (2010) 1–30, https://doi.org/10.1016/j.rser.2009.07.032.
[28] S. Bouadila, M. Lazaar, S. Skouri, S. Kooli, A. Farhat, Energy and exergy analysis of a new solar air heater with latent storage energy, Int. J. Hydrogen Energy 39 (2014) 15266–15274, https://doi.org/10.1016/J.IJHYDENE.2014.04.074.
[29] M.J. Huang, P.C. Eames, S. Mccormack, P. Griffiths, N.J. Hewitt, Micro-encapsulated phase change slurries for thermal energy storage in a residential solar energy system, Renew. Energy 36 (2011) 2932–2939, https://doi.org/10.1016/j.renene.2011.04.004.
[30] E. Bilgen, B.J.D. Bakeka, Solar collector systems to provide hot air in rural applications, Renew. Energy 33 (2008) 1461–1468, https://doi.org/10.1016/J.RENENE.2007.09.018.
[31] B.L. Evans, S.A. Klein, J.A. Duffie, A design method for active-passive hybrid space heating systems, Sol. Energy 35 (1985) 189–197, https://doi.org/10.1016/0038-092X(85)90010-6.
[32] A. Saxena, Varun, A.A. El-Sebaii, A thermodynamic review of solar air heaters, Renew. Sustain. Energy Rev. 43 (2015) 863–890, https://doi.org/10.1016/J.RSER.2014.11.059.
[33] A. El Khadraoui, S. Bouadila, S. Kooli, A. Farhat, A. Guizani, Thermal behavior of indirect solar dryer: nocturnal usage of solar air collector with PCM, J. Clean. Prod. 148 (2017) 37–48, https://doi.org/10.1016/J.JCLEPRO.2017.01.149.
[34] A. Reyes, L. Henríquez-Vargas, R. Aravena, F. Sepúlveda, Experimental analysis, modeling and simulation of a solar energy accumulator with paraffin wax as PCM, Energy Convers. Manag. 105 (2015) 189–196, https://doi.org/10.1016/J.ENCONMAN.2015.07.068.
[35] Heat and Cold Storage with PCM, Springer Berlin Heidelberg, Berlin, Heidelberg, 2008, https://doi.org/10.1007/978-3-540-68557-9.
[36] Y. Hu, P.K. Heiselberg, A new ventilated window with PCM heat exchanger—performance analysis and design optimization, Energy Build. 169 (2018) 185–194, https://doi.org/10.1016/j.enbuild.2018.03.060.
[37] C. Heiselberg, P. Kvols, O. Kalyanova, CLIMAWIN: Technical Summary Report, 2013. http://vbn.aau.dk/files/203815355/CLIMAWIN_Technical_Summary_Report.pdf. (Accessed 30 March 2018).
[38] F.P. Incropera, D.P. DeWitt, Fundamentals of Heat and Mass Transfer, J. Wiley, 2002.
[39] User's guide comsol multiphysics ®. www.comsol.com/support/knowledgebase. (Accessed 6 May 2019).